Bull. Mater. Sci. (2024) 47:130
https://doi.org/10.1007/s12034-024-03198-0

Triadic metal chalcogen $HgBi_2S_3$ nanoparticles as sensitizers for TiO_2 thin film: SILAR synthesis and characterization

SACHIN PADWAL[1,2,*], RAHUL WAGH[2], JIVAN THAKARE[3] and RAJENDRA PATIL[2]
[1]Science Department, Government Polytechnic Nashik, New Building Campus, Samangaon Road, Nashik 422101, India
[2]PSGVPM Arts Commerce and Science College, Shahada, Nandurbar 455409, India
[3]Energy and Environmental Research Center, Grand Forks, ND 58202-9018, USA
*Author for correspondence (sachin3380@gmail.com)

MS received 28 June 2023; accepted 22 December 2023

Abstract. The compound, mercury bismuth sulphide ($HgBi_2S_3$), represents a promising semiconductor within the II–V–VI group, demonstrating potential as a solar cell absorber layer. However, its synthesis and investigation through the successive ionic layer adsorption and reaction (SILAR) method have remained unexplored. This study focuses on the successful synthesis of $HgBi_2S_3$ nanoparticles using the SILAR technique atop wide band gap n-type semiconducting titanium dioxide (TiO_2) thin films. Characterization via X-ray diffraction (XRD) confirmed the synthesis, revealing an average crystallite size of 93.83 nm. The lattice strain percentage was measured at 0.1467 with a dislocation density of 1.13×10^{-4} 1/nm^2. Scanning electron microscopy (SEM) analysis showcased the spherical morphology of the nanoparticles, exhibiting average sizes of 169, 238 and 329 nm corresponding to 5, 10 and 15 SILAR cycles, respectively. The thickness of the $TiO_2/HgBi_2S_3$ composite thin film ranged from 12 to 18 μm. Notably, sensitizing the TiO_2 film with $HgBi_2S_3$ nanoparticles resulted in a substantial reduction in the contact angle by $\sim$24°. Optical studies demonstrated a significant decrease in the energy band gap of TiO_2 from 3.06 to 1.6 eV post-sensitization with $HgBi_2S_3$ nanoparticles, indicating enhanced light absorption capabilities. Interestingly, the energy band gap of the $TiO_2/HgBi_2S_3$ composite thin film remained consistent across different SILAR cycles. Moreover, electrochemical impedance spectroscopy and photoelectrochemical analyses revealed the intriguing performance characteristics of the $TiO_2/HgBi_2S_3$ composite thin film, showcasing promising yet marginal enhancements.

Keywords. SILAR; mercury bismuth sulphide; titanium dioxide; XRD; PEC; EIS.

1. Introduction

Although the world's electricity needs are in a state of flux, the International Energy Agency (IEA) reports that the worldwide demand for electricity was 23,200 terawatt-hours (TWh) in the year 2020. According to the 2020 report from the IEA, roughly 29% of the world's overall electricity production was sourced from non-conventional or renewable energy sources. The report does mention that solar energy is the fastest-growing source of renewable electricity, with a growth rate of 18% in 2020 [1]. IEA in its report published in 2020, enlists numerous advantages of energy generation using photovoltaic devices [2]. Photovoltaic cells are electronic devices that efficiently convert solar energy into electricity without emitting pollutants into the environment. These devices do not have any moving parts, making them low-maintenance. Silicon-based crystalline and amorphous solar panels have been effectively used to generate renewable power, but their efficiency is relatively low and their initial cost is high due to the expensive manufacturing process involved [3]. The fabrication of the first dye-sensitized solar cell (DSSC) was carried out by Regan and Gratzel in 1991 [4]. Following this significant milestone, researchers worldwide have shown great interest in DSSCs. A thin layer of titanium dioxide (TiO_2) coated with an organic or inorganic dye is the fundamental component of a DSSC [5,6]. When compared to smaller TiO_2 particles, larger particles are less efficient. The reason for this reduced efficiency is that larger particles tend to scatter light, and they are unable to effectively adsorb dye [7]. The efficiency of light absorption across the full visible spectrum is the reason why the sensitizer in a DSSC is crucial for maximum light collection [8]. DSSCs have utilized binary metal chalcogenide, including cadmium sulphide (CdS), cadmium selenide (CdSe), lead sulphide (PbS) and antimony sulphide (SbS) as sensitizers [9]. Until now, photovoltaic performance has been reported for synthesized ternary metal chalcogenide, such as copper bismuth sulphide (CuBiS), silver bismuth sulphide (AgBiS), copper indium sulphide (CuInS) and copper indium selenide

Published online: 17 June 2024

(CuInSe) [10–17]. Brower *et al* [18] synthesized mercury bismuth sulphide by heating the constituent elements in evacuated sealed silica glass tubes. Ubale and Shirbhate [19] utilized a chemical bath deposition method to produce HgS/Bi_2S_3 composite thin films, which were reported to have an optical energy band gap of 2.24 eV [19,20]. Various techniques have been attempted to deposit mercury suphide (HgS) for photovoltaic purposes, which has an energy band gap of ∼2.1 eV [21–24]. Several studies have reported the optical energy band gap and absorption coefficient of bismuth sulphide (Bi_2S_3) thin films to be between 1.2 and 1.84 eV and 10^5 cm^{-1}, respectively [25–29]. These properties make bismuth sulphide (Bi_2S_3) and mercury sulphide (HgS) and probably their composite thin films, a suitable choice for the absorber layer. In the domain of renewable energy investigation, mercury bismuth sulphide ($HgBi_2S_3$) has been surfaced as a largely unexplored, yet exceedingly promising substance. This compound, classified within the II–V–VI semiconductor group, exhibits an impressive optical band gap range of 1.4–1.7 eV. This distinctive attribute positions $HgBi_2S_3$ as an outstanding contender for applications in photovoltaics, offering superior light-absorption capabilities spanning between 10^4 and 10^5 cm^{-1}. Leveraging these optical characteristics within composite thin films holds significant promise for augmenting the light-capturing efficacy of solar cells. This pursuit is crucial in advancing more effective and sustainable photovoltaic technologies [30,31]. However, until now, triadic metal chalcogen of mercury bismuth sulphide ($HgBi_2S_3$) has not been synthesized or reported using successive ionic layer adsorption and reaction (SILAR) method. SILAR method is a simple and low-cost technique for deposition of good quality thin films. The properties of thin film deposited can be altered based upon molarity of solutions used, immersion and rinsing time and number of SILAR cycles [32]. In this study, we report, for the first time, the synthesis and characterization of the triadic metal chalcogen of mercury bismuth sulphide ($HgBi_2S_3$)-sensitized titanium dioxide (TiO_2) thin film through the SILAR method. In recent strides made in semiconductor materials for photovoltaic applications, the creation and analysis of TiO_2 thin films sensitized with $HgBi_2S_3$ mark an innovative trajectory. TiO_2, a widely recognized semiconductor material in the realm of photovoltaics, has enjoyed considerable attention. The successful amalgamation of $HgBi_2S_3$ and TiO_2 introduces a realm of possibilities, opening avenues for diverse semiconductor composite development with multifaceted applications. Aligned with established research methodologies, our study systematically investigates the impact of deposition time on the intrinsic properties of this composite. This facet holds paramount importance, facilitating precise customization of the material for specific applications. Extensive literature underscores that variations in deposition time serve as a pivotal parameter for optimizing thin film characteristics, tailoring them to the unique needs of various solar-cell technologies and optoelectronic applications. Our investigations indicate that the initial photovoltaic performance in this study lies within a moderately modest range, akin to analogous pioneering research initiatives. Despite these initially moderate outcomes, this research acts as a pivotal foundation for ongoing advancements in the field. By delving into the multifaceted factors influencing photovoltaic efficiency, our findings establish groundwork for future studies aimed at achieving heightened solar-cell performance. These endeavours bear significant importance as they hold the potential to yield cost-effective, high-efficiency solar cells. Successful advancements in this area would substantially bolster renewable energy production and diminish dependence on traditional fossil fuels [33,34].

2. Experimental

2.1 *Deposition of thin film of wide band gap n type semiconductor titanium dioxide (TiO_2) by spin-coating technique*

TiO_2 thin film was deposited on fluorine-doped tin oxide (FTO) glass substrate. The dimension of the FTO substrate used was L × B × W, 2.5 cm × 92.5 cm × 2.2 mm. This FTO substrate was first washed carefully with lab-grade detergent and then, rinsed with double-distilled water (DDW). Post-drying in air, the substrate was subjected to ultra violet (UV) light for 30 min to enhance adhesion of the film. The sol–gel for TiO_2 was prepared by using precursors containing 2 g of TiO_2 powder (25 nm particle size, Degussa, Germany), 12 ml of 60% ethanol, 2 ml of acetyl acetone (assay 98%) and 1 ml nitric acid (assay 68–70%). These precursors were stirred at room temperature for 10 h using magnetic stirrer. The final sol–gel was white coloured thick viscous fluid. For deposition of thin film, the sol–gel was imbued evenly over the unified FTO substrate. The FTO substrate was then pirouetted with a speed of 900 rpm for about 60 s. Excess sol–gel hurled away giving thin and uniformly coarse film of TiO_2 over entire FTO substrate. Figure 1 depicts the schematic for spin-coating technique and SILAR method for thin film deposition. The thin film was then dried in air for 10 min. The resulting thin film was free from any defects, such as cracks and comets. To augment the crystallinity of the film, it was normalized at 400°C for 30 min in a muffle furnace with temperature escalation of 100°C per 30 min. Post-annealing, the colour of the TiO_2 thin film was lighter shade of white with excellent adhesion with FTO substrate.

2.2 *Sensitization of thin film of TiO_2 with triadic metal chalcogen mercury bismuth sulphide ($HgBi_2S_3$) nanoparticles*

To sensitize TiO_2 thin film with $HgBi_2S_3$ nanoparticles, mercury chloride ($HgCl_2$) served as the antecedent for Hg^{+1}ions, bismuth nitrate pentahydrate ($Bi(NO_3)_3{\cdot}5H_2O$)

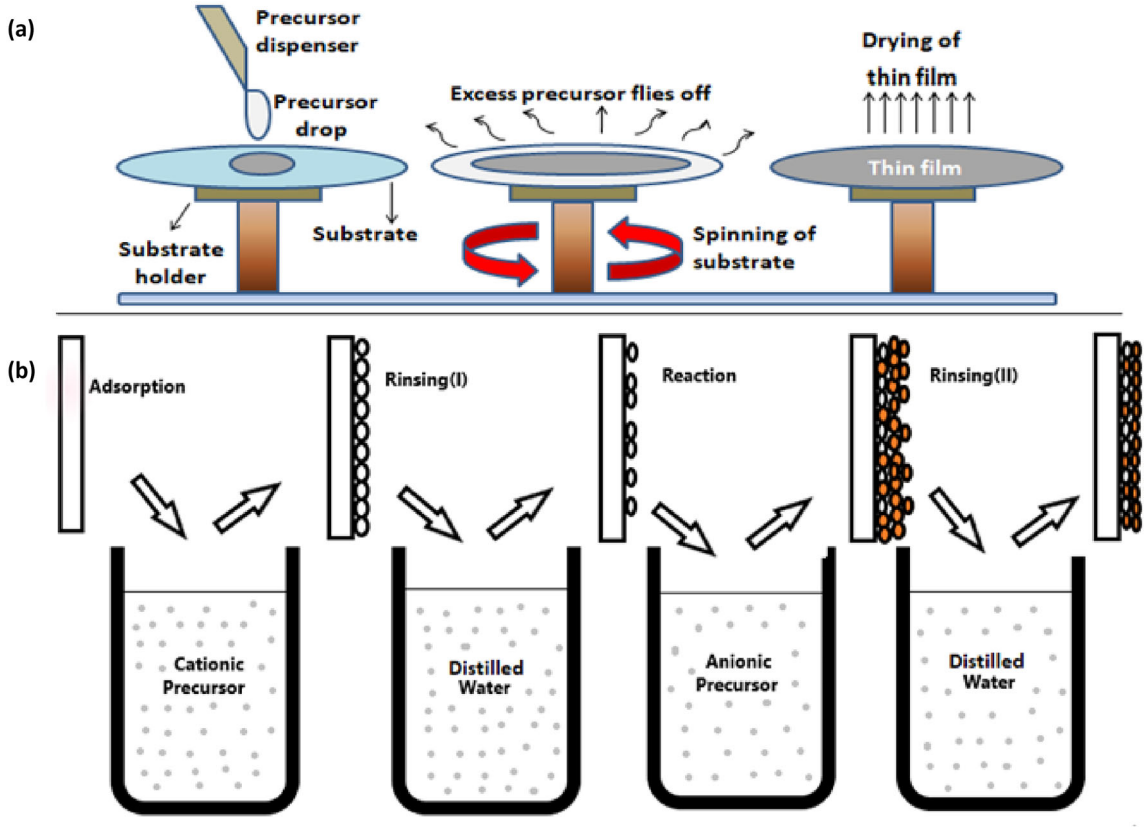

Figure 1. Schematic diagram for (**a**) spin-coating technique and (**b**) successive ionic layer adsorption and reaction (SILAR) method for deposition of thin films.

served as the antecedent for Bi^{+3}ions and thioacetamide (CH_3CSNH_2) served as the antecedent for S^{-2} ions. All the precursor solutions used for sensitization process had uniform molarity of 0.1 M. One SILAR cycle incorporated the following steps:

- Immersion of TiO_2 thin film shellacked FTO substrate into 0.1 M $HgCl_2$ aqueous solution (pH ∼ 7) for 20 s,
- Rinsing this TiO_2/Hg^{+1} impregnated thin film-coated FTO substrate in distilled water for 10 s,
- Immersion of TiO_2/Hg^{+1} impregnated thin film-coated FTO substrate in 0.1 M $Bi(NO_3)_3{\cdot}5H_2O$ solution dissolved in 10% triethanolamine (TEA, pH ∼ 8–9) for 20 s,
- Rinsing this $TiO_2/Hg^{+1}/Bi^{+3}$ impregnated thin film-coated FTO sub strate in distilled water for 10 s,
- Immersion of $TiO_2/Hg^{+1}/Bi^{+3}$ impregnated thin film-coated FTO substrate in 0.1 M CH_3CSNH_2 aqueous solution (pH ∼ 7–8) for 20 s,
- Rinsing this $TiO_2/Hg^{+1}/Bi^{+3}/S^{-2}$ impregnated thin film-coated FTO substrate in distilled water for 10 s.

The reaction eventuating in above SILAR cycle can be explained as follows, Here, $HgCl_2$ and $Bi(NO_3)_3{\cdot}5H_2O$ function as oxidizing agents, whereas CH_3CSNH_2 functions as reducing agent. Both $HgCl_2$ and $Bi(NO_3)_3{\cdot}5H_2O$ are reduced to form elemental mercury and bismuth sulphide, respectively. The CH_3CSNH_2 is oxidized to form the disulphide and acetamide. Nitric acid is also a byproduct of the reaction. After completing coveted number of SILAR cycles, the film was desiccated in air. With expansion in number of SILAR cycles, the colour of the film gradually reformed from a light grey-brown hue to a darker shade of grey-brown implying upsurge in thickness of the film deposited as shown in figure 2. Composite film of $TiO_2/HgBi_2S_3$ was synthesized with number of SILAR cycles equal to 5, 10 and 15 as shown in figure 2. This $TiO_2/HgBi_2S_3$ composite film was then, normalized at 200°C for 30 min and then, cooled to room temperature in the course of time by means of muffle furnace. The rationale behind selecting a relatively thicker sensitizer layer, ranging from 5 to 15 μm, was attributed to the absence of prior studies or established knowledge regarding the functionality and efficacy of the particular sensitizer in question. Given the novelty and lack of precedent for this specific sensitizer, a strategy employing varying numbers of SILAR cycles—specifically, 5, 10 and 15 cycles—was undertaken. This approach was chosen to systematically explore the potential influence of different sensitizer thicknesses on the resulting composite's characteristics and performance. The intent was to comprehensively assess and understand the effects of these variable thicknesses as potential

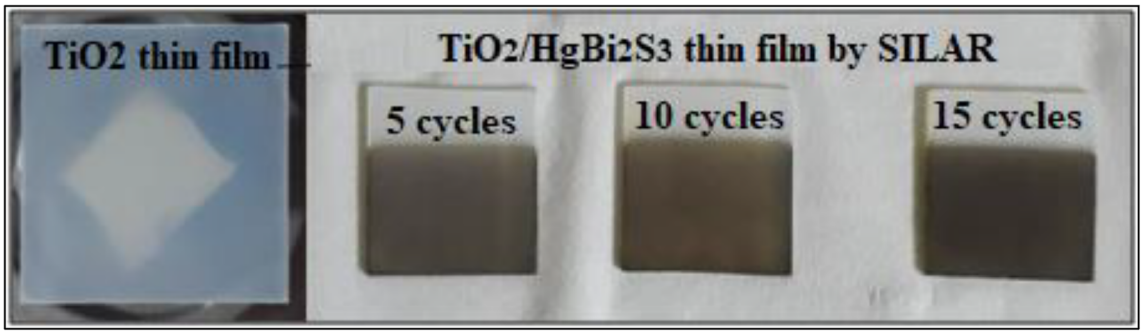

Figure 2. Thin film of TiO_2 deposited by spin-coating technique and $TiO_2/HgBi_2S_3$ aggregate film by SILAR method with 5, 10 and 15 cycles.

sensitizing layers, given the absence of established guidelines or precedents within existing literature regarding the optimal thickness for this particular sensitizer in the context of the described application.

3. Characterization techniques

The structural investigation of $TiO_2/HgBi_2S_3$ aggregate thin film was carried out using X-ray diffractometry (XRD) by means of an automated Bruker D8 advanced X-ray diffractometer with a diffraction angle of 20–80°. The Scherrer formula was used to determine the average crystallite size of the film. An optical absorption study was carried out using a Jasco UV–visible spectrophotometer (V 630) in the wavelength range from 200 to 800 nm at room temperature. The optical energy band gap was determined from the Tauc graph of $(h\nu)$ *vs.* $(\alpha h\nu)^2$. Surface morphological and cross-sectional investigations were studied with a scanning electron microscope (SEM) attached with an energy dispersive spectrometer (EDS) detector (Quanta 200 ESEM, The Netherlands). Electrochemical impedance spectroscopy (EIS) was recorded with the help of potentiostat/galvanostat (IVIUM Vertex model). Photoelectrochemical (PEC) performance was investigated using 3A steady state solar simulator SS-F5-3A (Enli Technology Co., Taiwan). And the contact angle was measured with the help of a lab-made facility consisting of a high-definition 16 megapixel Sony IMX471 camera.

4. Results and discussion

4.1 *Structural studies*

To study structural properties of $TiO_2/HgBi_2S_3$ aggregate film, XRD pattern was recorded. The recorded XRD pattern along with matched standard reference COD code is shown in figure 3a–e. Being a triadic metal chalcogen, the peaks in the XRD pattern incorporate peaks for TiO_2, Hg and Bi_2S_3. With regard to TiO_2, the maximum intensity peak is recorded at 2θ equal to 27.44° from (1 1 0) diffraction plane, which matches up with standard reference COD code (96-900-4142) (space group = P 42/m n m; space group number = 136; lattice parameter *a*, *b* and *c* = 4.5930, 4.5930 and 2.9590 Å respectively; calculated density = 4.25 g cm^{-3}; volume of cell = 62.42 10^6 pm^3; RIR = 3.72) as shown in figure 3 [35]. As per this matched COD code, the TiO_2 thin film has rutile phase and tetragonal crystal structure. Significant peaks are recorded at 2θ equal to 54.32 and 36.07° corresponding to diffraction from the (2 1 1) and (1 0 1) planes, respectively.

Regarding Hg, the XRD pattern is similar to standard reference COD code (96-151-2512) (space group = I 4/m m m; space group number = 139; lattice parameter *a*, *b* and *c* = 3.8620, 3.8620 and 3.7910 Å, respectively; calculated density = 11.78 g cm^{-3}; volume of cell = 56.54 10^6 pm^3; RIR = 24.18), which confirms tetragonal crystal system [36]. The most intense peak is noticed at 2θ equal to 33.08° from diffraction plane (1 0 1). Other prominent peaks are at 2θ equal to 32.76 and 58.69° corresponding to the diffraction planes (1 1 0) and (2 1 1), respectively. Pertaining to Bi_2S_3, the XRD pattern cognates with standard reference COD code (96-900-7400) (space group = P n m a; space group number = 62; lattice parameter *a*, *b* and *c* = 11.1360, 3.9570 and 11.0350 Å, respectively; calculated density = 7.02 g cm^{-3}; volume of cell = 486.26 10^6 pm^3; RIR = 3.93), which implies orthorhombic crystal structure [37]. The maximum intensity peak in the pattern is located at 2θ equal to 28.87° with respect to diffraction from (1 1 2) plane. Similarly, other intense peaks are recorded at 2θ equal to 25.29 and 25.48° for the diffraction planes of (3 0 1) and (1 0 3), respectively.

This validates synthesis of polycrystalline $HgBi_2S_3$ thin film by SILAR method onto *n* type wide band gap TiO_2 thin film. The synthesis of this triadic compound by incorporating elements known for their tetragonal and orthorhombic crystal structures, showcases the diverse and intricate nature of crystallographic arrangements involved in forming the complex structures. Examination via XRD confirmed the crystalline nature of the synthesized compound, manifesting distinctive diffraction patterns that align with the

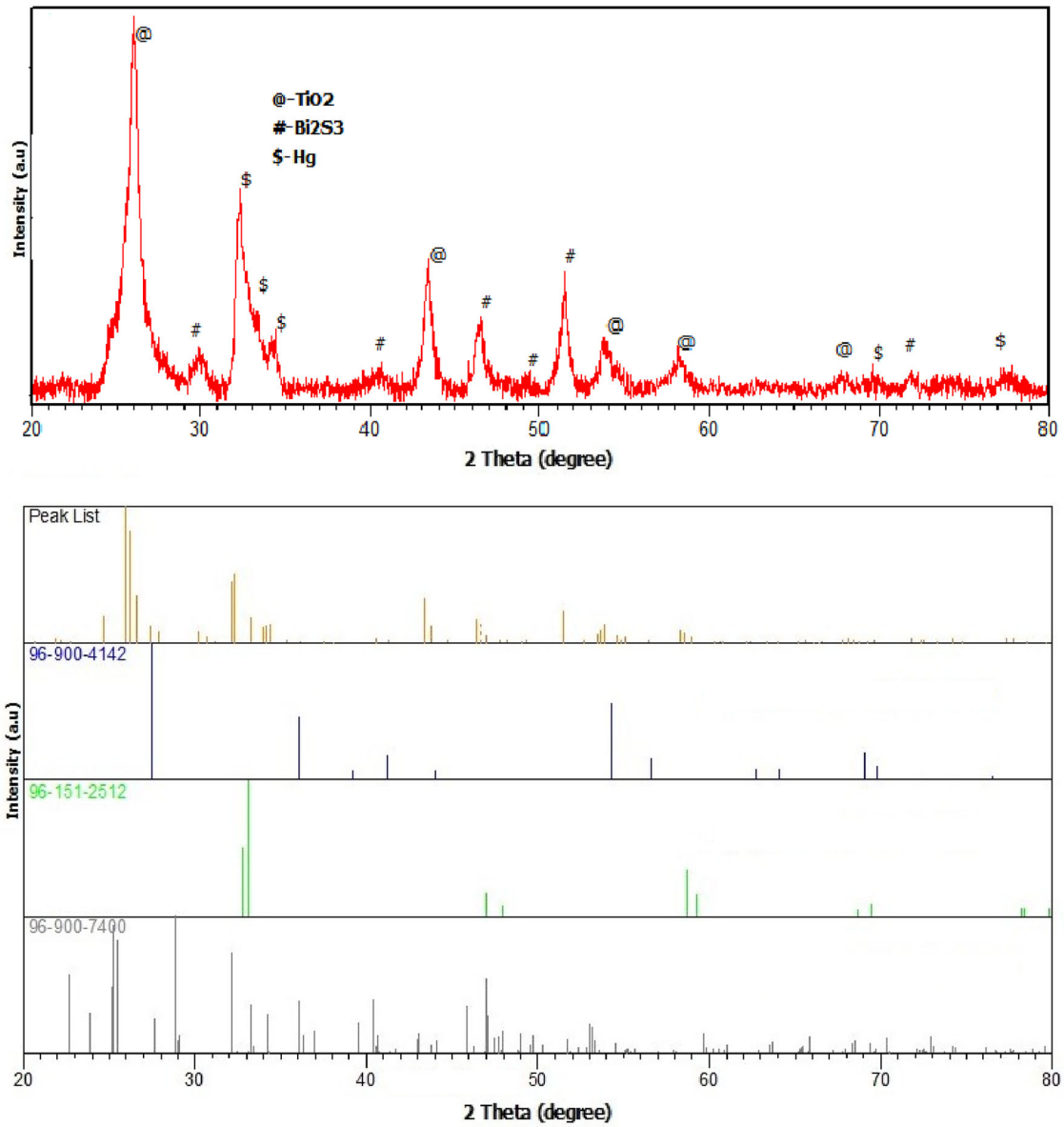

Figure 3. XRD pattern for (**a**–**b**) $TiO_2/HgBi_2S_3$ aggregate film by SILAR (5 cycles) annealed at 200°C. (**c**) Reference COD code (96-900-4142) for TiO_2. (**d**) Reference COD code (96-151-2512) for Hg. (**e**) Reference COD code (96-900-7400) for Bi_2S_3.

presence of both tetragonal and orthorhombic crystal systems. These XRD findings serve as robust evidence attesting to the successful production of a polycrystalline thin film composed of $HgBi_2S_3$, a triadic metal chalcogen, through the utilization of the SILAR method atop a spin-coated TiO_2 thin film.

In the exploration of the sensitization process employing the $HgBi_2S_3$ sensitizer in conjunction with TiO_2 thin films, an initial investigation centred on evaluating specific parameters, namely, the average crystallite size, average lattice strain percentage and dislocation density limited to five SILAR cycles. This approach facilitated an initial appraisal of this innovative amalgamation. The deliberate focus on five cycles was aimed at laying the groundwork for a more extensive inquiry. This preliminary analysis of five SILAR cycles aimed to establish a fundamental understanding of the impact of sensitization process on the properties of TiO_2 thin films, serving as a foundational platform for subsequent investigations across varying cycle numbers. The average crystallite size (D) of the $TiO_2/HgBi_2S_3$ aggregate film was computed using Scherrer formula given by equation (1) [38]:

$$D = \frac{0.9\lambda}{d\cos\theta}, \tag{1}$$

where λ is the wavelength of X-ray (CuKα radiation = 0.154 nm), θ the Bragg diffraction angle and β the full width half maximum of the XRD peaks appearing at

different angle θ. Average crystallite size was identified as 93.83 nm for $TiO_2/HgBi_2S_3$ aggregate thin film. Average lattice strain percentage (ε) was calculated using equation (2). For the $TiO_2/HgBi_2S_3$ aggregate thin film, it was equal to 0.1467 and the dislocation density (δ) for $TiO_2/HgBi_2S_3$ aggregate film was determined using equation (3) was equal to 1.13×10^{-4} 1/nm^2 [39].

$$\varepsilon = \frac{\beta \cos\theta}{4}, \tag{2}$$

$$\delta = \frac{1}{D^2} \tag{3}$$

where D is average crystallite size. Diminutive significance of dislocation density connotes excellent crystallinity of the thin film [40].

4.2 *Morphological studies*

Morphological studies of the TiO_2 and $TiO_2/HgBi_2S_3$ aggregate thin film was executed by means of SEM. Figure 4 represents surface morphology and cross-section micrograph for TiO_2 thin film (figure 4a and e) and $TiO_2/HgBi_2S_3$ aggregate thin film (figure 4b–d and 4f–h), respectively. Regarding TiO_2 thin film, the FTO substrate is deposited with mesoporous layer of TiO_2 nanoparticles (particle size 25 nm, Degussa, Germany). Nanopores can be seen unvaryingly strewed over the substrate. These nanopores will enhance percolation of liquid electrolyte through TiO_2 thin film hence, improving charge transmission towards the conducting FTO layer. The thickness of TiO_2 thin film as perceived from cross-section micrograph is about 10–11 μm with standard deviation of 0.30 μm. Taking into account of this value of standard deviation, it can be said that the thickness of the TiO_2 thin film is consistent across unified domain of the FTO substrate.

In case of $TiO_2/HgBi_2S_3$ aggregate thin film, the surface morphology shows spherical nanoparticles distributed over TiO_2 thin film. As the number of SILAR cycles are expanded from 5 to 15, the interlaced gorge and ridge pattern of nanoparticles seems to quilt over the entire TiO_2 thin film. Spherical shape of nanoparticles can be easily traced out from the micrograph for 15 SILAR cycles. The surface texture of $TiO_2/HgBi_2S_3$ aggregate thin film is very poriferous, which will allow smooth channel for permeation of liquid electrolyte for better charge transmission [41]. The thickness of aggregate thin film expands with SILAR cycles. The thickness of the film varies from about 12–18 μm as seen in figure 4. Acknowledging the thickness of TiO_2 thin film, it can be noticed that the thickness of $HgBi_2S_3$ thin film deposited is ranging from 1 to 7 μm as the number of SILAR cycles are increased from 5 to 15. Spherical nature of nanoparticles deposited can also be recognized from cross-section micrograph. The overall standard deviation in aggregate film thickness is computed about 0.27 μm for all SILAR cycles. Thus, this implies consonant thickness film synthesized from SILAR method.

The three-dimensional (3D) surface projection for TiO_2 thin film and $TiO_2/HgBi_2S_3$ aggregate film for 5, 10 and 15 SILAR cycles is represented in figure 5 The topography of TiO_2 thin film is very much persistent over entire FTO substrate. The distribution of mounds and gorges can be noticed cohesively throughout the thin film. There is no direct exposure to FTO substrate across entire film. The heights of mounds are very much identical signifying equal

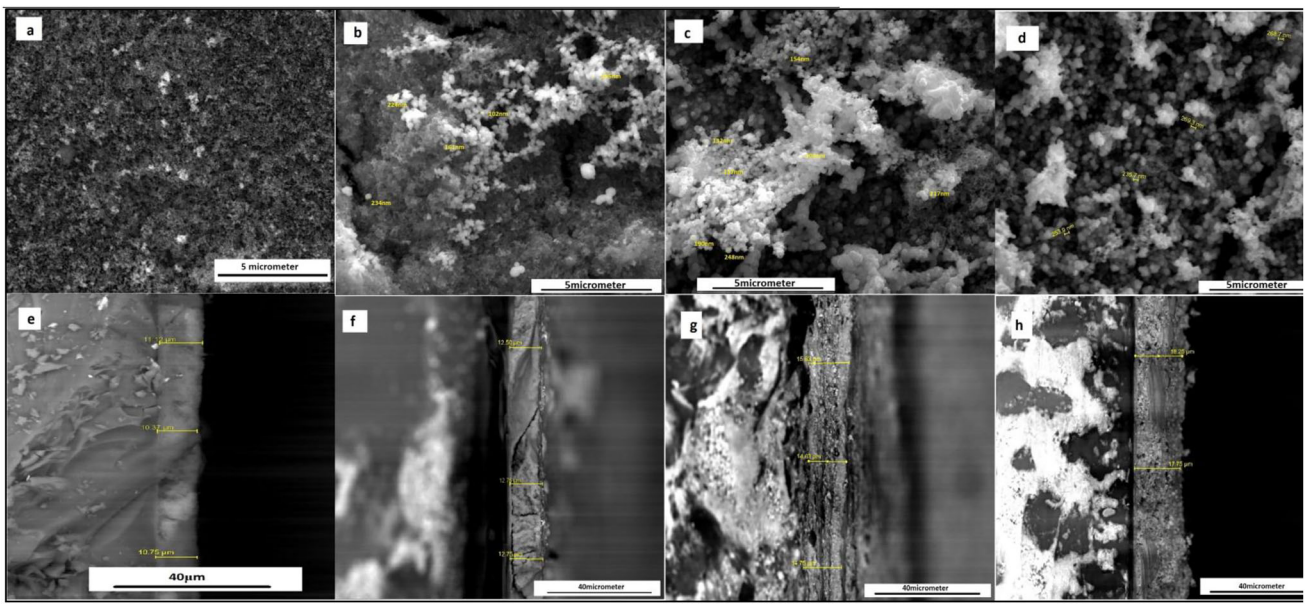

Figure 4. Surface morphology and cross-sectional micrograph of TiO_2 thin film (**a** and **e**) and $TiO_2/HgBi_2S_3$ aggregate thin film (**b–d** and **f–h**) for 5, 10 and 15 SILAR cycles, respectively.

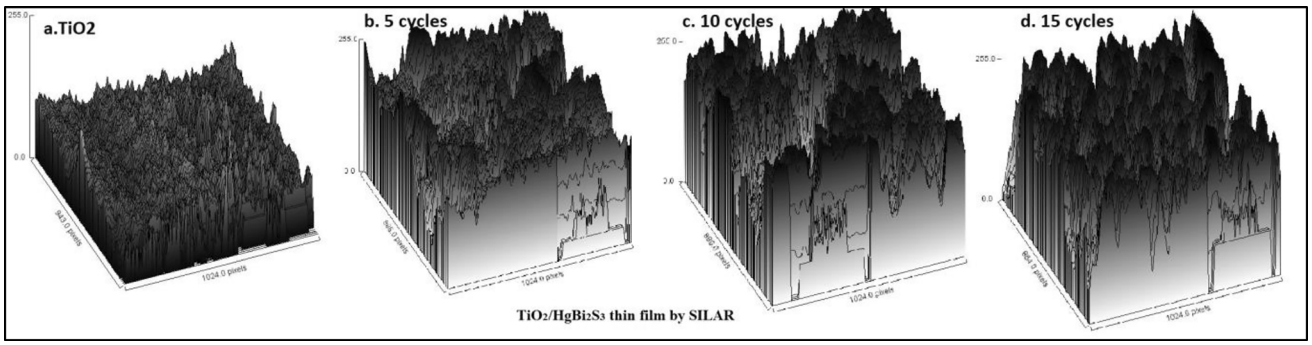

Figure 5. 3D surface projection for TiO_2 thin film and $TiO_2/HgBi_2S_3$aggregate thin film for 5, 10 and 15 SILAR cycles.

thickness of TiO_2 thin film. There are no rapid changes in elevation of mounds implying smaller values of gradient throughout the thin film. Regarding $TiO_2/HgBi_2S_3$ aggregate thin film, the topography of surface is again mounds and gorges. The depth of gorges goes on increasing with SILAR cycles making the film more porous. Overall, the elevation of mounds is expanding with SILAR cycles signifying increase in thickness of the deposited thin film. The value of gradient is marginal as noticed from figure 5.

The average particle size histogram for $TiO_2/HgBi_2S_3$ aggregate film for 5, 10 and 15 SILAR cycles is shown in figure 6. The average particle size was computed using specialized software across 5, 10 and 15 SILAR cycles. It was estimated about 169, 238 and 329 nm, respectively, for the three SILAR cycles. This clearly conveys gradual increase in particle size with increasing number of SILAR cycles. For five SILAR cycles, majority of particle size varies in the range of 130–200 nm, while for 10 SILAR cycles, it is between 165 and 235 nm. And for 15 SILAR cycles, the particle size varies from 250 to 370 nm. The particle size distribution is narrow for five SILAR cycles, whereas broader for 10 and 15 SILAR cycles as noticed from histogram in figure 6.

Wettability studies of TiO_2 thin film and $TiO_2/HgBi_2S_3$ aggregate film for 5, 10 and 15 SILAR cycles shows appreciable depreciation in contact angle as exhibited in figure 7. Equal number of drops of distilled water were placed on thin films and contact angle was measured with the help of software. The contact angle was found to be about 33–34° for distilled water/TiO_2 thin film interface. This value of contact angle reduced by about 23–24° to reach a value of about 9–10° for distilled water/TiO_2/$HgBi_2S_3$ aggregate film interface for 5, 10 and 15 SILAR cycles. The value of contact angle for aggregate film is

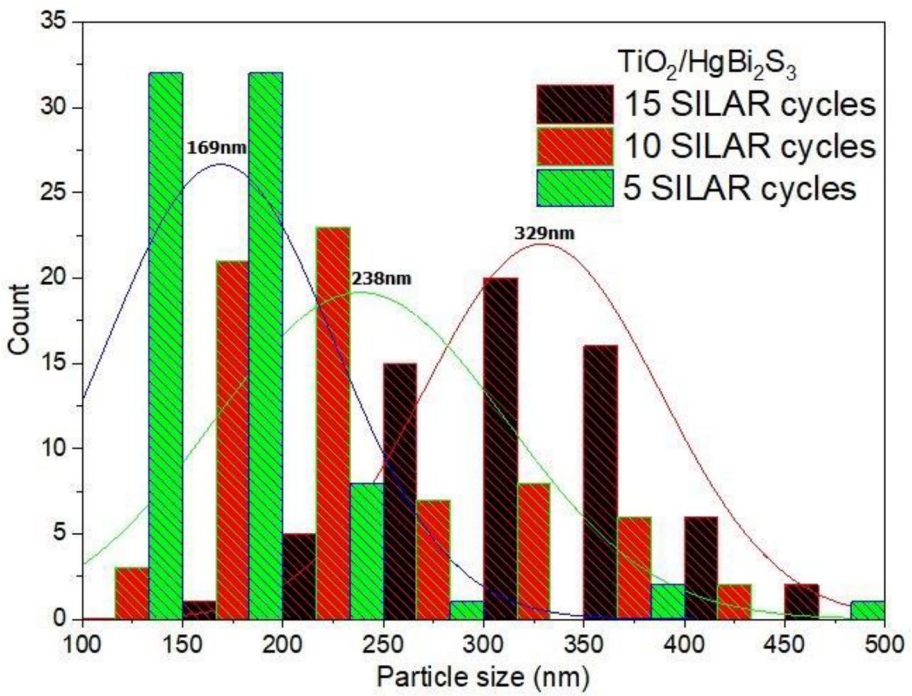

Figure 6. Average particle size histogram $TiO_2/HgBi_2S_3$ aggregate thin film for 5, 10 and 15 SILAR cycles.

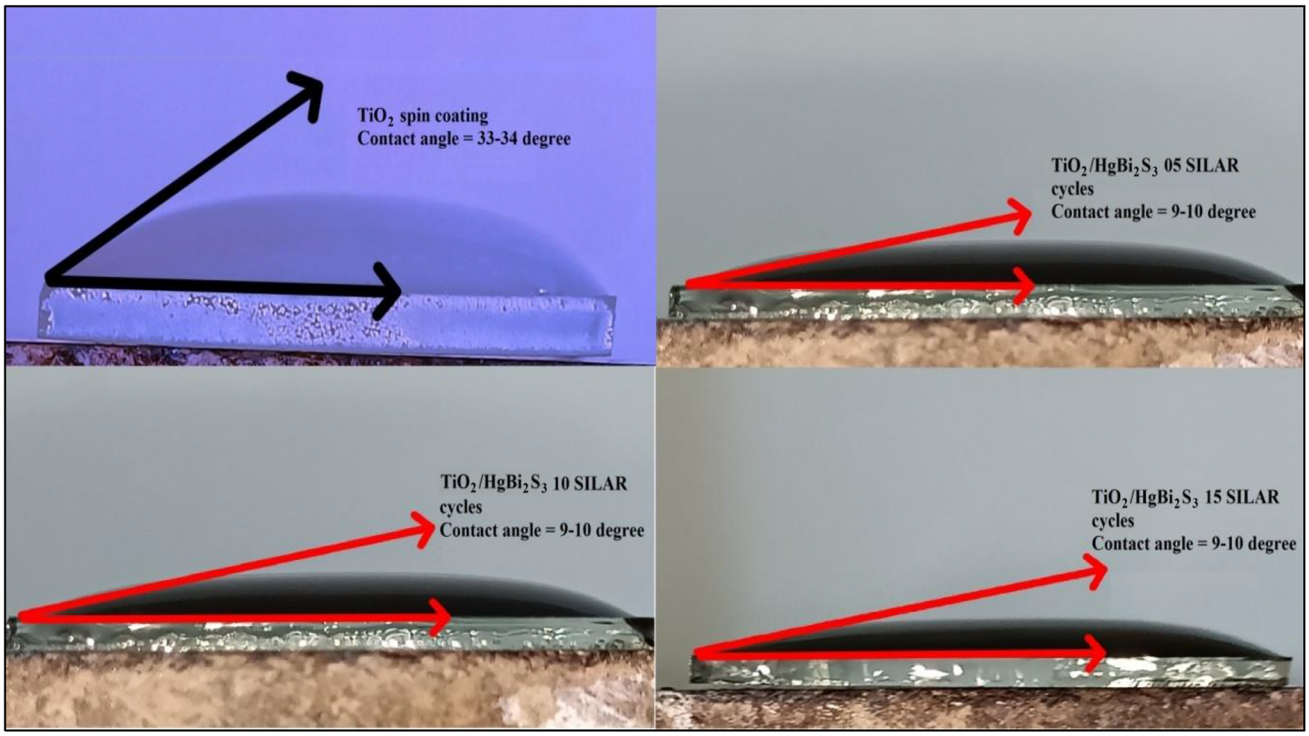

Figure 7. Contact angle for TiO_2 thin film and $TiO_2/HgBi_2S_3$ aggregate thin film for 5, 10 and 15 SILAR cycles. Significant depreciation in contact angle from 33 to 10°.

independent of number of SILAR cycles as seen in figure 7. Lower values of contact angle for $TiO_2/HgBi_2S_3$ aggregate film conveys good adhesion between thin film and water and hence, water-based electrolyte. The decline in contact angle indicates upsurge in hydrophilic nature of thin film, which would subsequently elevate the dissemination of electrolyte and charges transfer [42].

4.3 *Elemental studies*

With a view to execute elemental studies of $TiO_2/HgBi_2S_3$ aggregate film, energy dispersive X-ray spectroscopy (EDXS) was accomplished. A variety of regions across each thin film, produced using 5, 10 and 15 SILAR cycles, was deliberately selected to conduct thorough elemental analysis, guaranteeing a comprehensive assessment of the film's composition. The EDXS spectrum of $TiO_2/HgBi_2S_3$ aggregate film for 5, 10 and 15 SILAR cycles is shown in figure 8. Each film deposited by SILAR cycles was randomly scanned for elemental studies. Presence of spectral response for Ti, O, Hg, Bi and S in the EDXS spectrum confirms the synthesis of $TiO_2/HgBi_2S_3$ aggregate film. This finding demonstrates the inherent stability of the elemental composition throughout the deposition procedure, thereby confirming the deliberate and uniform control of synthesis parameters. The percentage of each element detected in each SILAR cycle is represented in figure 8. Percentage of Hg, S and O seems to be almost consistent in the film, whereas the percentage of Bi and Ti has changed moderately with number of SILAR cycles. Since the percentage of Hg is on higher side, the thin film can be considered opulent with respect to Hg. Small amounts of Si and Cl are detected in EDXS spectrum, which arise from FTO substrate on which the thin film is deposited. In conclusion, the EDXS elemental analysis confirms the significant impact of the deposition process, particularly the quantity of SILAR cycles, on the elemental makeup of the composite. This meticulous evaluation highlights the careful control of synthesis parameters, facilitating the cohesive incorporation of Hg and Bi_2S_3 nanoparticles into the TiO_2 matrix. This integration enhances specific properties of the resulting thin films. The systematic changes in elemental composition emphasize the complex relationship between deposition conditions and structure of the resulting film.

4.4 *Optical studies*

Absorbance plots of TiO_2 thin film and $TiO_2/HgBi_2S_3$ aggregate film for 5, 10 and 15 SILAR cycles, as a function of wavelength of incident light is shown in figure 9. The absorbance of TiO_2 thin film is at the peak in the wavelength range of 200–325 nm. Beyond this, the absorbance of TiO_2 thin film declines sharply with the lowest absorbance at 400 nm. Further, there is gradual upsurge in absorbance

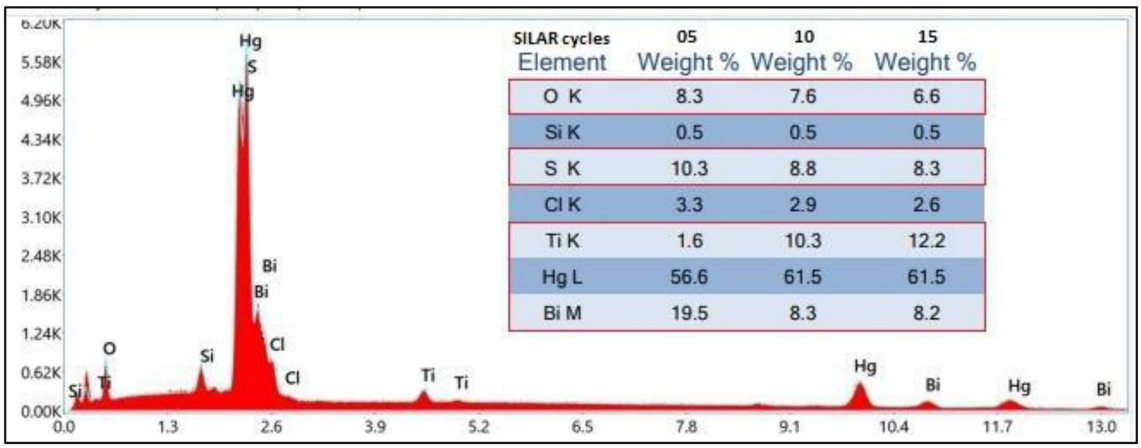

SILAR cycles	05	10	15
Element	Weight %	Weight %	Weight %
O K	8.3	7.6	6.6
Si K	0.5	0.5	0.5
S K	10.3	8.8	8.3
Cl K	3.3	2.9	2.6
Ti K	1.6	10.3	12.2
Hg L	56.6	61.5	61.5
Bi M	19.5	8.3	8.2

Figure 8. Energy dispersive X-ray spectroscopy (EDXS) studies for $TiO_2/HgBi_2S_3$ aggregate thin film for 5, 10 and 15 SILAR cycles.

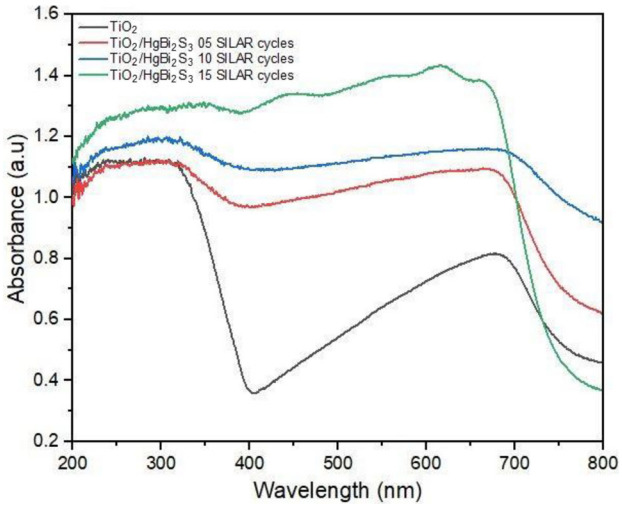

Figure 9. Absorbance plot of TiO_2 thin film and $TiO_2/HgBi_2S_3$ aggregate thin film for 5, 10 and 15 SILAR cycles.

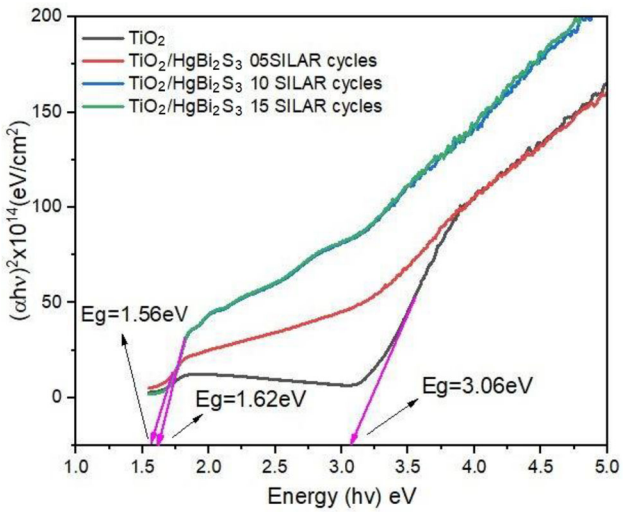

Figure 10. Optical energy band gap of TiO_2 thin film and $TiO_2/HgBi_2S_3$ aggregate thin film for 5, 10 and 15 SILAR cycles.

with second maxima at around 690 nm and again the plot shows sharp fall in the absorbance of TiO_2 thin film. The UV absorbance spectrum of TiO_2 thin film displayed dual peaks, indicating distinct phenomena at different wavelength ranges. The primary absorbance peak, observed between 200 and 325 nm, signifies the band gap excitation characteristic of TiO_2, followed by a sharp decline due to the reduced photon energy beyond the band gap. Additionally, a secondary absorbance peak around 690 nm suggests an alternate mechanism, possibly related to surface states, defects, or impurities, contributing to localized absorbance in the visible/near-infrared spectrum. This observation suggests that the dual absorbance peaks reflect specific phenomena operating at different wavelengths rather than conflicting characteristics.

After deposition of $HgBi_2S_3$ nanoparticles upon TiO_2 thin film, the absorbance plot exhibits major transition in absorbance behaviour of aggregate film. The absorbance of aggregate film shows perceptible change as seen in figure 9. The absorbance of aggregate film shows consistent enhancement in entire visible range as well as near infra-red range of the spectrum. Identical behaviour is exhibited by aggregate film in the case of all SILAR cycles. Slightly higher absorbance is noticed in case of aggregate thin film for 15 SILAR cycles as compared with other cycles. There is sharp fall in absorbance beyond 700 nm wavelength of incident light. Thus, this elevation in absorbance of light by $TiO_2/HgBi_2S_3$ aggregate film may have impact on its photovoltaic abilities [43].

Figure 10 represents the computation of optical energy band gap using Tauc plot method [44]. It is an important tool to study absorption spectrum of thin films. It can be used to determine optical energy band gap of materials. y-axis of the plot represents $(\alpha h\nu)^2$ in (eV cm^{-2}) as a function of energy ($h\nu$) of the incident light in eV. The band

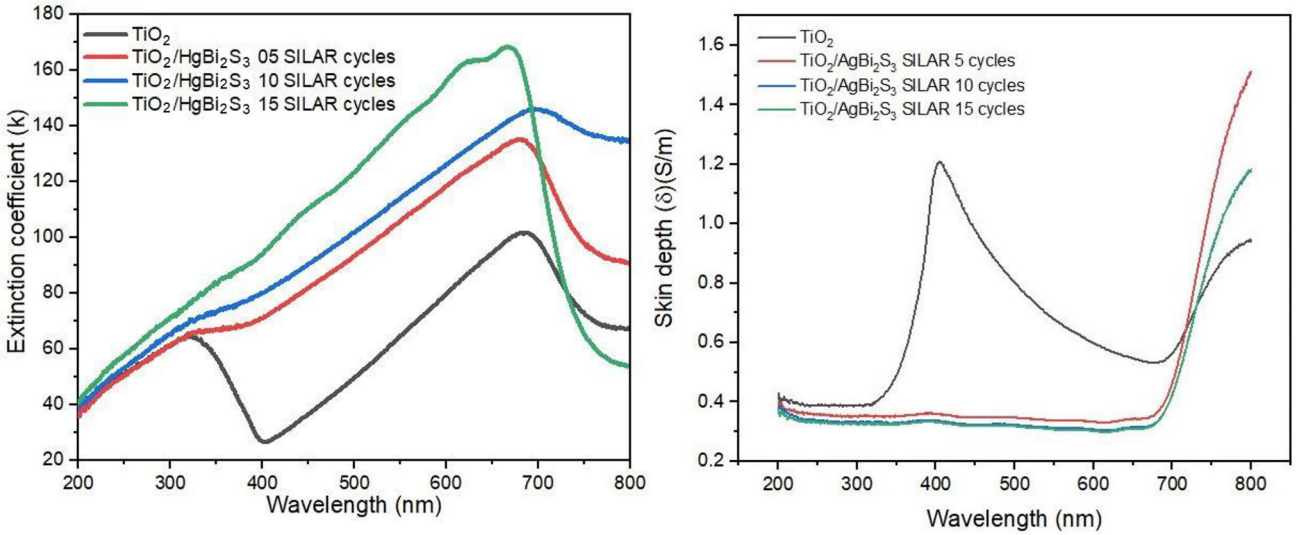

Figure 11. Extinction coefficient (k) and skin depth (δ) of TiO_2 thin film and $TiO_2/HgBi_2S_3$ aggregate thin film as a function of wavelength of incident light for 5, 10 and 15 SILAR cycles.

gap of TiO_2 thin film determined here, using Tauc plot is about 3.06 eV, which corresponds with already established theoretical and experimental results. When this thin film of TiO_2 is stimulated with $HgBi_2S_3$ nanoparticles by SILAR method, the band gap of resulting aggregate film denigrates almost by $\sim$1.5 eV to fulfil the value of 1.56–1.62 eV as noticed in the figure. This denigration of optical energy band gap validates the findings of absorbance spectra discussed above that the aggregate thin film absorbs considerable amount of incident light. The value of band gap is unperturbed by number of SILAR cycles as seen in the plot. Thus, gradual expansion in thickness of $HgBi_2S_3$ thin film over TiO_2 thin film does not degrade absorption of light. On the contrary, it is independent of thickness of $HgBi_2S_3$ thin film. The downside in value of optical energy band gap of aggregate thin film may enhance the process of charge transfer at the $TiO_2/HgBi_2S_3$ interface [45].

Variation in extinction coefficient (k) and skin depth (δ) as a function of wavelength of incident light is shown in figure 12. Extinction coefficient is the criteria for absorption of light by thin film at a specific wavelength [46] and skin depth is the criteria for how deep the light penetrates into the thin film prior to getting attenuated [47]. Extinction coefficient of $TiO_2/HgBi_2S_3$ aggregate thin film reveals sharp increase till it attains maxima at around 650–675 nm. The aggregate thin film absorbs maximum incident light irrespective of number of SILAR cycles around the wavelength of 650–675 nm. Further, the coefficient and hence, absorption downfalls sharply as noticed in figure 12. Regarding skin depth of $TiO_2/HgBi_2S_3$ aggregate thin film as noticed from figure 11, the value of skin depth is almost consistent irrespective of number of SILAR cycles. It forms plateau like structure parallel to wavelength axis in the plot till almost 700 nm. Beyond 700 nm, the skin depth experiences sharp rise, which suggests that the thin film has become transparent to light [48]. This sharp rise in skin depth also suggest change in electrical properties of thin film for specific wavelength [49].

4.5 *EIS studies*

EIS studies were carried out to investigate charge transfer resistance at various interfaces of device fabricated with and

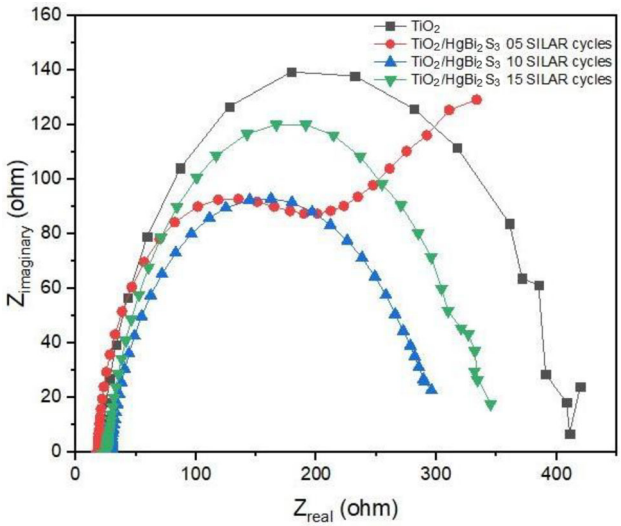

Figure 12. Nyquist plot for TiO_2 and $TiO_2/HgBi_2S_3$ aggregate thin film device fabricated for 5, 10 and 15 SILAR cycles with polysulphide electrolyte.

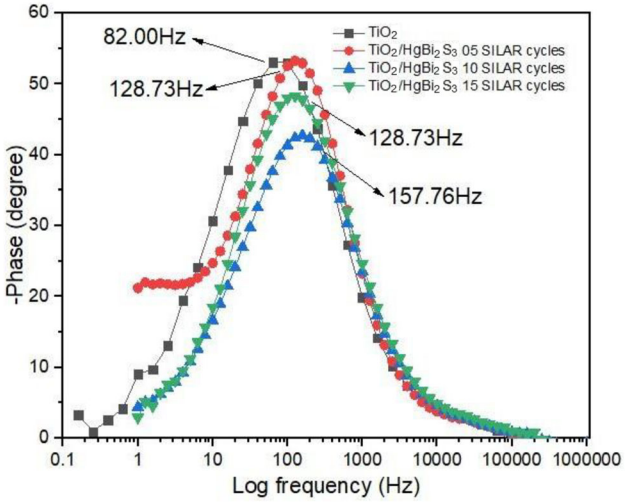

Figure 13. Nyquist plot for TiO_2 and $TiO_2/HgBi_2S_3$ aggregate thin film device fabricated for 5, 10 and 15 SILAR cycles with polysulphide electrolyte.

without $HgBi_2S_3$ dye molecule in the following combination:

FTO/TiO_2/ $HgBi_2S_3$/polysulphide electrolyte/ carbon electrode/FTO

The polysulphide electrolyte was prepared in ethanol and distilled water as solvent with ratio of 8:2. Sulphur powder of 1 M and sodium sulphide of 1 M were added to above solvent and stirred at room temperature for 10 min using magnetic stirrer. Sodium hydroxide (NaOH) of 1 M was mixed with the above precursor, which serves as a base to dissolve sulphur. NaOH also helps to maintain pH of the electrolyte, which is essential for stability of performance of the device [50]. This precursor solution was stirred for 15 min at room temperature to dissolve all the powder. The electrolyte was then filtered to remove any undissolved solid matter. The resulting electrolyte was transparent golden yellow coloured liquid. This electrolyte was introduced in above mentioned sandwiched combination of electrodes and dye nanoparticles. The modulation signal of 5 mV ranging from 1 Hz to 1 MHz was applied to the combination under dark condition for 5, 10 and 15 SILAR cycles. The results of test are shown as Nyquist plot in figure 12. Nyquist plot consists of real and imaginary parts of impedance of the fabricated device on x- and y-axes, respectively.

For FTO/TiO_2/polysulphide electrolyte/carbon electrode/FTO combination, the plot is represented by single semicircle having the largest radius among all tested devices. This insinuates higher charge transfer resistance and recombination resistance at carbon electrode/polysulphide electrolyte interface [51]. Regarding FTO/TiO_2/$HgBi_2S_3$/polysulphide electrolyte/carbon electrode/FTO combination, only five SILAR cycle-device have semicircle followed by line at low frequency region. For all cycles, the radius of semicircles is on higher side stating higher values of charge transfer and recombination resistance at counter electrode and electrolyte interface. This significant value of resistance will limit photovoltaic performance of the device. For five-cycle device, the Nyquist plot exhibits semicircle followed by line, which indicates diffusion-restricted behaviour of the electrolyte. This diffusion-restricted behaviour of electrolyte can be due to scarce diffusion of the polysulphide electrolyte in the mesoporous structure of TiO_2 photo electrode. It can hence, causes less access of polysulphide electrolyte to the TiO_2 nanoparticles and limits the photovoltaic ability of the device [52].

Figure 13 shows Bode plot for all fabricated devices as explained earlier. The variation in phase is from 0 to 60° as a function of log of frequency in the range of 1 Hz–1 MHz. In the plot, the high inclination of all the curves indicates that the devices have high phase lag. This phase lag can be due to reasons, such as high resistance of the device or sluggish charge transfer between the electrolyte and TiO_2 electrode [53]. This ultimately affects the efficiency of the fabricated device. The crests in the plot can be used to estimate electron lifetime (τ) with the help of equation (4) [54]:

$$\tau = \frac{1}{2\pi f}. \tag{4}$$

Table 1. Electron lifetime for TiO_2 and $TiO_2/HgBi_2S_3$ aggregate thin film device fabricated for 5, 10 and 15 SILAR cycles with polysulphide electrolyte.

Combination	Cycles	Maximum frequency from Bode plot (Hz)	Electron lifetime (ms)
FTO/TiO_2/polysulphide electrolyte/carbon electrode/FTO	Without $HgBi_2S_3$ as dye	82	1.94
FTO/TiO_2/$HgBi_2S_3$/polysulphide electrolyte/carbon electrode/FTO	5	128.73	1.23
	10	128.73	1.23
	15	157.76	1.00

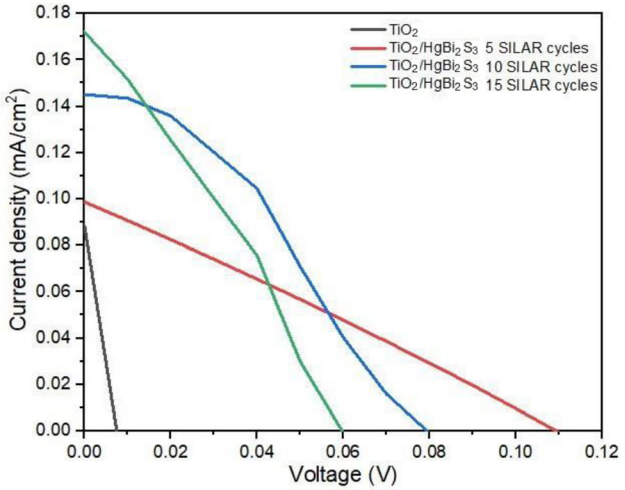

Figure 14. Current density (*JV*) plot for TiO_2 and $TiO_2/HgBi_2S_3$ aggregate thin film device fabricated for 5, 10 and 15 SILAR cycles with polysulphide electrolyte.

where *f* is the maximum frequency for a curve from Bode plot. The details of electron lifetime estimated from Bode plot is enlisted in table 1.

4.6 *PEC studies*

PEC studies of the device fabricated with and without $HgBi_2S_3$ as dye were executed with the following combination:

FTO/TiO_2/$HgBi_2S_3$/polysulphide electrolyte/
carbon electrode/FTO

The results of the studies are represented in figure 14 for 5, 10 and 15 SILAR cycles. The current density plot as a function of applied voltage is shown in the figure. The detailed findings of PEC studies are tabulated in table 2. Marginal photovoltaic activity is exhibited by TiO_2/$HgBi_2S_3$ aggregate thin film fabricated device. Device with 10 SILAR cycles exhibits maximum efficiency amount of all the devices. Further increase in SILAR cycles deteriorates efficiency of the device. The selection of a relatively thick sensitizer layer (5–15 μm) composed of $HgBi_2S_3$ stemmed from the absence of prior studies utilizing $HgBi_2S_3$ as a sensitizer for TiO_2 in PEC applications. This investigation represents an inaugural attempt to explore the potential of $HgBi_2S_3$ as a sensitizer, aiming to pioneer research efforts in this unexplored domain. The rationale behind choosing the thickness range of 5–15 μm was primarily driven by the novelty of employing $HgBi_2S_3$ as a sensitizer in TiO_2-based PEC systems. Given the dearth of precedent studies or established guidelines regarding the optimal sensitizer thickness, the selection was exploratory in nature. It aimed to ascertain the sensitizer's efficacy across a range of thicknesses and evaluate its potential in enhancing the PEC performance of TiO_2.

Table 2. Photovoltaic studies of TiO_2 and $TiO_2/HgBi_2S_3$ aggregate thin film device fabricated for 5, 10 and 15 SILAR cycles with polysulphide electrolyte.

Device combination	SILAR cycles	Sun	Area (cm^2)	I_{sc} (mA)	V_{oc} (V)	P_{max} (mW)	I_{max} (mA)	V_{max} (V)	Efficiency	Fill factor	J_{sc} (mA/cm^2)
FTO/TiO_2/polysulphide electrolyte/carbon electrode/FTO	Without $HgBi_2S_3$ as dye	1	0.5	0.0442	0.00747	0	0.0442	0	0	0	0.0884
FTO/TiO_2/$HgBi_2S_3$/polysulphide electrolyte/carbon electrode/ FTO	5	1	1	0.0987	0.1093	0.0028	0.0477	0.06	0.0028	26.54	0.0987
	10	1	1	0.1451	0.0794	0.0041	0.1045	0.04	0.004	36.26	0.1451
	15	1	1	0.1719	0.05970	0.0030	0.0756	0.04	0.003	29.45	0.171

5. Conclusions

In the present work, we have successfully demonstrated simple technique to synthesize triadic metal chalcogen $HgBi_2S_3$ nanoparticles-sensitized TiO_2 thin film by SILAR method. The SILAR method is simple low-cost method to synthesize good quality thin film with uniform thickness. The thickness of the thin film can be controlled by number of SILAR cycles. XRD studies confirmed deposition of polycrystalline $HgBi_2S_3$ thin film over wide band gap semiconducting TiO_2 thin film. The study of the particle shape revealed that the nanoparticles had a spherical morphology, and they were deposited in the form of very thin film over the FTO substrate. The thickness of $HgBi_2S_3$ thin film increased with number of SILAR cycles. Elemental studies substantiated synthesis of intended elements in the thin film with consistent percentage in all SILAR cycles. The hydrophilic nature of the TiO_2 thin film experiences notable enhancement subsequent to the deposition of $HgBi_2S_3$, emphasizing discernible interfacial alterations. Optical studies revealed absorbance of $HgBi_2S_3$-sensitized TiO_2 thin film exhibited significant upsurge with downfall in optical energy band gap from 3.06 to 1.62 eV. This value of band gap is very close to the best suited band gap of 1.39 eV for solar-cell absorber layer. EIS studies revealed high charge transfer resistance at various interfaces, which subsequently affected photovoltaic performance of the device fabricated. $HgBi_2S_3$-sensitized TiO_2 thin film showcased marginal photovoltaic ability. The selection of a thicker sensitizer layer and varied SILAR cycle numbers were motivated by the pioneering nature of this research endeavour in the domain of $HgBi_2S_3$ as a sensitizer for TiO_2 in PEC applications, aiming to pave the way for future investigations and advancements in this field. Taking into account all these properties of $HgBi_2S_3$-sensitized TiO_2 thin film, our future work will be directed in the same direction.

Acknowledgements

We sincerely acknowledge the Kaviyatri Bahinabai Chaudhari North Maharashtra University Jalgaon, Department of Physics, PSGVP Mandal's Arts, Commerce & Science College Shahada, Nandurbar, Advanced Physics Lab, Department of Physics, Savitribai Phule University, Pune, Baburaoji Gholap Science College, Pune and Icon Analytical, New Mumbai, for providing characterization facilities.

References

[1] International Energy Agency (2022) World Energy Outlook 2022 IEA Paris. Retrieved from https://www.iea.org/reports/world-energy-outlook-2022
[2] International Energy Agency (2020) Renewables 2020 IEA Paris. Retrieved from https://www.iea.org/reports/renewables-2020
[3] Frass L and Partain, 2010 *Solar cells and their applications* (2nd edn.) (USA: A John Wiley & Sons Inc., Publication)
[4] O'Regan B and Grätzel M 1991 *Nature* **353** 737
[5] Poortmans J and Arkhipov V 2006 *Thin film solar cells—Fabrication, characterization and application* (England: Wiley Series in Material for electronic and optoelectronics applications)
[6] Park N G, Kim K M, Kang M G, Ryu K S, Chang S H and Shin Y J 2005 *Adv. Mater.* **17** 2349
[7] Jeng M J, Wung Y L, Chang L B and Chow L 2013 *Int. J. Photoenergy,* Article ID 563897
[8] Ikpesu J E, Iyuke S E, Daramola M and Okewale A O 2020 *Sol. Energy* **206** 918
[9] Mane R S and Lokhande C D 2000 *Mater. Chem. Phys.* **65** 1
[10] Coughlan C, Ibáñez M, Dobrozhan O, Singh A, Cabot A and Ryan K 2017 *Chem. Rev.* **117** 5865
[11] Pai N, Lu J, Senevirathna D C and Anthony S J 2018 *J. Mater. Chem. C* **6** 2483
[12] Zhou S, Yang J, Li Z W, Jiang Q, Luo Y, Zhang D *et al* 2016 *J. Electrochem. Soc.* **163** D63
[13] Huang P C, Yang W C and Lee M W 2013 *J. Phys. Chem. C* **117** 18308
[14] Xu S, Cheng N, Yin H, Cao D and Mi B 2020 *Chem. Eng. J.* **397** 125463
[15] Samsi N S, Effendi N A S, Zakaria R and Ali A M M 2017 *Mater. Res. Express* **4** 044005
[16] Li Y, Wei Y, Feng K, Pei H Y and Sun Bao J 2018 *Mater. Res. Express* **5** 065903
[17] Yang J, Kim J Y, Yu J H, Ahn T Y, Lee H, Choi T S *et al* 2013 *Phys. Chem. Chem. Phys.* **15** 20517
[18] Brower W S, Parker H S and Roth R S 1973 *Mater. Res. Bull.* **8** 859
[19] Ubale A U and Shirbhate S C 2010 *J. Alloys Compd.* **497** 228
[20] Rincón M E, Sánchez M, George P J, Sánchez A and Nair P K 1998 *J. Solid State Chem.* **136** 167
[21] Wagh R A, Kulkarni A N, Baviskar P K, Pathan H M and Patil R S 2018 *Mater. Renew. Sustain Energy* **7** 3
[22] Barthaburu M, Pérez I G, Aguiar I, Bentos Pereira H, Bethencourt L and Paulo B 2017 *Nano-Struct. Nano-Objects* **10** 15
[23] Xu X and Carraway E R 2012 *Nanomater. Nanotechnol.* **2** 17
[24] Patil R S, Lokhande C D, Mane R S, Pathan H M, Joo O S and Han S H 2006 *Mater. Sci. Eng. B* **129** 59
[25] Pineda E, Nicho M E, Nair P K and Hu H 2012 *Sol. Energy* **86** 1017
[26] Liao H C, Wu M C, Jao M H, Chuang C M, Chen Y F and Su W F 2012 *CrystEngComm* **14** 3645
[27] Nikam P R, Baviskar P K, Sali J V, Gurav K V, Kim J H and Sankapal B R 2015 *Ceram. Int.* **41** 10394
[28] Arumugam J, George A, Raj A D, Irudayaraj A A, Josephine R L, Sundaram S J *et al* 2021 *J. Alloys Compd.* **5** 158681
[29] Rajalakshmi P U, Oommen R and Sanjeeviraja C 2011 *Chalcogenide Lett.* **8** 683
[30] Yao J D, Zheng Z Q and Yang G W 2019 *Prog. Mater. Sci.* **100573**
[31] Jia Z, Righetto M, Yang Y, Xia C Q, Li Y *et al* 2023 *ACS Energy Lett.* **8** 1485
[32] Soonmin H 2022 Encyclopedia. Publ., Retrieved from https://encyclopedia.pub/entry/26528
[33] Zhang X, Grätzel M and Hua J 2016 *Front. Optoelectron.* **9** 3
[34] Zhao H and Rosei F 2017 *Chem. Cell Press* **3** 229
[35] Meagher E P and Lager G A 1979 *Canad. Mineral.* **17** 77

[36] Lejaeghere K, Van Speybroeck V, Van Oost G and Cottenier S 2014 *Crit. Rev. Solid State Mater. Sci.* **39** 1
[37] Lundegaard L F, Makovicky E, Boffa Ballaran T and Balic Zunic T 2005 *Phys. Chem. Miner.* **32** 578
[38] Cullity B D 1978 *Elements of X-ray diffractions* (2nd edn.) (USA: Addision-Wisley Publishing Company Inc.)
[39] Kaltenhauser V, Rath T, Haas W and Torvisco 2013 *J. Mater. Chem. C* **1** 7825
[40] Islam M A, Hossain M S, Aliyu M M, Chelvanathan P, Huda Q, Karim M R *et al* 2013 *Energy Procedia* **33** 203
[41] Tachibana Y, Moser J E, Gratzel M, Klug D R and Durran J R 1996 *J. Phys. Chem. B* **100** 20056
[42] Lukong V T, Mouchou R T, Enebe G C, Ukoba K and Jen T C 2022 *Mater. Today Proc.* **62** S63
[43] Liu J, Li S, Li J, Zhang L, Li Y and Wang Y 2015 *J. Mater. Sci.: Mater. Electron.* **26** 8766
[44] Tauc J 1968 *Mater. Res. Bull.* **3** 37
[45] Kaniyoor A, Ramaprabhu S and Maiti P K 2008 *J. Phys. Chem. C* **112** 4653
[46] Nemade K R 2017 *Russ. J. Non-Ferr. Met.* **58** 82
[47] Abu El Hiaja A J 2001 *Opt. Appl.* **31** 739
[48] Sami Chiad 2015 *Int. Lett. Chem. Phys. Astron.* **45** 50
[49] Benramache S, Aoun Y, Lakel S and Benhaoua B 2019 *Mater. Res. Express* **6** 126418
[50] Prasad R, Tamboli M B, Bhalekar P S, Kadam V P, Abraham V, Rajesh J T *et al* 2018 *Mater. Res. Express* **5** 066208
[51] MacDonald J R 1987 *Ann. Biomed. Eng.* **15** 297
[52] Iftikhar H, Sonai G G, Hashmi S G, Nogueira A F and Lund P D 2019 *Materials* **12** 1998
[53] Srinivasa Rao S, Punnoose D, Venkata Tulasivarma C, Pavan Kumar C H S S, Gopi C V V M and Kim S K 2015 *Dalton Trans.* **44** 2447
[54] Majumder S 2016 *Electrochim. Acta* **222** 100